JGR Planets

RESEARCH ARTICLE

Key Points:

- Detailed geomorphological-structural analysis of Ménec Fossae has been conducted, using imaging and newly processed topographic data
- Ménec Fossae has been shaped by transtensional tectonic activity, potentially related to the emplacement of a shallow water reservoir
- The hypothesis that shallow water reservoirs are widely distributed within Europa's ice shell is strengthened

Correspondence to:
P. Matteoni,
pietro.matteoni@fu-berlin.de

Ménec Fossae on Europa: A Strike-Slip Tectonics Origin Above a Possible Shallow Water Reservoir

Pietro Matteoni[1] , Alicia Neesemann[1], Ralf Jaumann[1], Jon Hillier[1], and Frank Postberg[1]

[1]Planetary Sciences and Remote Sensing, Institute of Geological Sciences, Freie Universität Berlin, Berlin, Germany

Abstract Faults and fractures may emplace fresh material onto Europa's surface, originating from shallow reservoirs within the ice shell or directly from the subsurface ocean. Ménec Fossae is a region of particular interest as it displays the interaction of several geological features, including bands, double ridges, chaotic terrains, and fossae, within a relatively small area. These features might affect the emplacement of buried material and subsequent exposure of fresh volatiles, prime targets for the upcoming *JUICE* and *Europa Clipper* missions in order to assess Europa's astrobiological potential. Previous studies have already revealed that a deep central trough is present at Ménec Fossae, flanked by several subparallel minor troughs and by a few asymmetrical scarps with lobate planforms. The presence of such features has motivated this study, given its potential to provide clear indications on the tectonic regime involved. Through detailed geomorphological-structural mapping using *Galileo* Solid State Imager data and terrain analysis on Digital Terrain Models, we could develop a novel hypothesis on the formation mechanisms that might have been involved in the study area. We propose that Ménec Fossae has been shaped by transtensional (strike-slip with an extensional component) tectonic activity, as indicated by the orientation and relationship of the tectonic features present. Likely, such transtensional tectonism occurred above or associated with shallow subsurface water, consistent with the overall morphology and topography of the study area and the presence of chaotic terrains and double ridges. These results strengthen the case for widely distributed shallow water reservoirs within Europa's ice shell.

Plain Language Summary Tectonic cracks, which can originate from shallow water bodies within the icy crust or directly from the subsurface ocean, may emplace fresh material onto Europa's surface. This kind of material is a prime target for upcoming space missions to assess Europa's habitability. We investigated the area of Ménec Fossae, which is characterized by many different geological features and structures within a relatively small area and can therefore provide clues on the mechanisms that shaped it. Our analyses were based on imaging and new topographic data, we developed a new hypothesis involving a combination of different tectonic styles as the driving processes for the formation of this area. This kind of tectonic activity could be related to a liquid water pocket located at a shallow depth within Europa's icy crust, which might explain the concurrent presence of some particular geological features in the area. These findings strengthen the case for the wide distribution of shallow water pockets distributed within the icy crust, which could allow future space missions to more easily assess Europa's habitability.

1. Introduction

Among the three possible Jovian ocean worlds, Europa, Ganymede, and Callisto, the most detailed and convincing evidence for an internal ocean has been obtained for Europa (e.g., Nimmo & Pappalardo, 2016). Not only does the magnetic induction response to Jupiter's time-varying magnetic field indicate the existence of a subsurface salty ocean (Khurana et al., 1998; Kivelson et al., 2000), but the moon's surface also shows indications of interaction with a liquid layer beneath the ice crust. Images from Voyager 2 and Galileo show a fractured icy surface, with regions where ice crust blocks seem to have moved in a slushy or liquid medium (Carr et al., 1998; Pappalardo et al., 1999). The orientations of some large-scale linear features also seem to have changed over time, implying rotation of the ice shell and a very low viscosity layer between the interior and the surface (Pappalardo et al., 1998). The thickness and thermo-physical structure of the ice shell are poorly constrained, models suggest it may be 20–30 km thick (e.g., Howell, 2021; Hussmann, 2002; Quick & Marsh, 2015), with a layer of warm, convecting ice underlying a cold, rigid crust (Barr & Pappalardo, 2005; Pappalardo et al., 1998). Additionally, analyses of surface features have given constraints on the thickness of the ice shell (e.g., Schenk, 2002; Singer et al., 2021).

Pressures at the base of the internal global ocean are too low for the formation of high-pressure ice phases, and the ocean is thus believed to be in contact with the rocky interior (Anderson et al., 1998). This raises the possibility of rich chemical exchange between the silicate interior and the subsurface ocean, perhaps via hydrothermal vents, and potentially chemical heating through serpentinization (Vance et al., 2007, 2016). Since long-lived radioactive elements are expected to be present in silicates, as they are within Earth's crust, a further source of energy that heats the rocky interior is radioactive decay (Běhounková et al., 2021; Hussmann et al., 2010). However, the major heating source is provided by tidal dissipation due to Europa's eccentric orbit, maintained over long time periods by orbital resonances with Io and Ganymede (Schubert et al., 2009; Sotin et al., 2009). These considerations make Europa one of the main candidates in the Solar System for supporting the development of life (Greenberg et al., 2000; Greenberg & Geissler, 2002). If biosignatures are produced within Europa's ocean, they will need to reach the surface to be detected by the upcoming Jupiter Icy Moons Explorer (*JUICE*) and *Europa Clipper* missions. There are indications of salts at some surface locations (e.g., Dalton et al., 2005; Trumbo et al., 2019b), consistent with recent extrusions or ejections of salt-rich liquid water from the moon's interior. However, these salts may also be directly incorporated within the ice shell and do not necessarily require water injection (Buffo et al., 2020). Some investigators have recently suggested that the salt minerals present on Europa's surface may be dominated by endogenic chlorinated species (e.g., sodium and/or magnesium chlorides), rather than by sulfates (Trumbo et al., 2017, 2019a, 2019b, 2022; Hand & Carlson, 2015; Ligier et al., 2016), which were the main previously hypothesized compounds (e.g., Dalton et al., 2012; Hansen & McCord, 2008; McCord et al., 1999; Orlando et al., 2005), with radiolysis producing the observed reddish-brown coloration of *lineae* and *chaos* regions. A chloride-rich, sulfate-poor ocean would likely be indicative of ongoing water/rock interaction at the seafloor, whereas a sulfate-rich and chloride-poor ocean could indicate either a primordial leached composition or significant cycling with the ice shell and delivery into the ocean of radiolytically produced sulfates (Hand et al., 2022).

At global scales, landform evolution on atmosphereless bodies is primarily driven by impact gardening, tectonics, and (cryo-)volcanism. Crater density and frequency analysis indicate that Europa's geologically active surface (Greenberg & Geissler, 2002; Greenberg et al., 1998) is relatively young (∼40–90 My, Bierhaus et al., 2009) with a wide variety of landforms including ridges, troughs, bands, lenticulae, and chaotic terrains (Greeley et al., 2000, 2004). To understand which resurfacing processes are responsible for Europa's anomalously young surface age, several compressional mechanisms have been invoked, such as subduction (cold, brittle, and dense outer portions of the ice shell sink into the underlying convecting warmer ice, in analogy to Earth's convergent plate boundaries; Kattenhorn & Prockter, 2014) and regional scale folding (e.g., Prockter & Pappalardo, 2000). Nevertheless, the tectonic regime that dominates within the ice shell is extensional, a hypothesis supported by numerous lines of evidence, such as the widespread presence of dilational bands that represent >40% of the total surface area (Kattenhorn & Hurford, 2009). Several types of geological features generated within such a tectonic regime, including bands, double ridges, cycloids, chaotic terrains, and fossae, might affect the emplacement of buried material and subsequent exposure of fresh volatiles on Europa's surface. We hereafter provide a general description for each of these types of geological features, which include the main terrains found in the study area (see Section 3.1).

Bands (Figure 1a), on Europa, are tabular zones of dilation in the ice shell where new crustal material intruded between the walls of a crack (Kattenhorn & Hurford, 2009); they have lengths of hundreds of km and widths of a few km up to ∼30 km. Bands are thought to represent a phenomenon analogous to Earth's mid-ocean ridge spreading centers, potentially making them the only other known feature in the Solar System where complete lithospheric separation has occurred (Kattenhorn & Prockter, 2014; Nimmo et al., 2003).

Double ridges (Figure 1b) are the most common tectonically related feature on Europa, comprising a central crack or trough flanked by two quasi-symmetric raised edifices, up to a few hundred meters high and less than 5 km wide (Kattenhorn & Hurford, 2009). The associated ridge features may extend for hundreds of kilometers and include some of the oldest features visible on the surface, with frequent cross-cutting implying numerous formation cycles over Europa's history. Numerous double ridges follow cycloidal paths (i.e., chains of arcs) across the surface: as the tidal stress field changes through time, propagation of tensile cracks occurs (Greenberg & Sak, 2014). Double ridges may indicate intrusions of near-surface liquid water (Dombard et al., 2013; Johnston & Montési, 2014), shear heating (Han & Showman, 2008; Kalousová et al., 2016; Nimmo & Gaidos, 2002), eruptions (Fagents, 2003), or direct extrusion of recently frozen ocean water by fractures opening and closing under tidal stresses (Greenberg et al., 2003). More recent studies suggest how double ridges might be formed through refreezing, pressurization, and fracturing of shallow water reservoirs (e.g., Culberg et al., 2022).
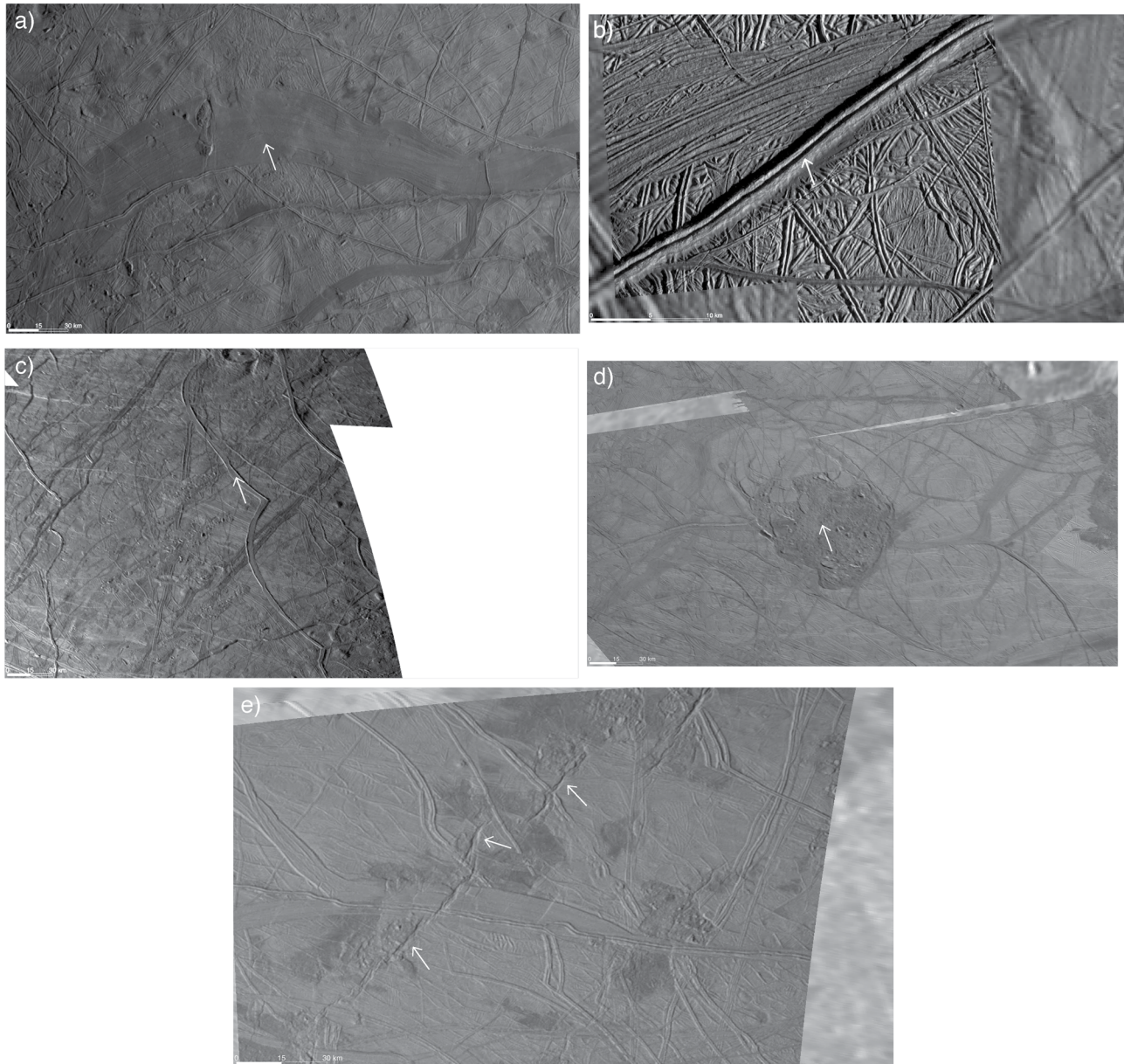
Figure 1. Examples of several geological features on Europa. White arrows indicate each terrain type described in the text: (a) Band (panel centered at 6°S, 122°E); (b) Double ridge (panel centered at 14°N, 86°E); (c) Cycloid (panel centered at 53°N, 73°W); (d) Chaos (panel centered at 46°S, 178°E); (e) Fossa (panel centered at 43°N; 5°E). North is up in all panels.

Cycloids (Figure 1c) are linked arcuate fractures that form hundreds to thousands of kilometers long chains of multiple concatenated segments (Kattenhorn & Hurford, 2009). Cycloids likely form as the principal tidal stresses on Europa change, either in response to daily (e.g., Greenberg et al., 1998) or other changes in the principal stress (Kattenhorn, 2004). A crack forms as the tidal stress in a given region increases and eventually exceeds the failure strength of the ice (i.e., becomes more tensile). A cycloidal path can track the changes in stress orientation with time as it propagates across Europa's surface if the crack propagates slowly (a few km/h). When the tidal stress decreases, propagation ceases, completing an arc (Rhoden et al., 2021).

Chaotic terrains are (Figure 1d), on Europa, geologically very young and extensively disrupted surface features, interpreted as reflecting recent interaction with shallow subsurface material (Chivers et al., 2021; Collins & Nimmo, 2009; B. E. Schmidt et al., 2011). Leading-hemisphere chaos regions have recently been shown to be compositionally distinct from their surroundings, probably indicating contributions from endogenous sodium chloride sourced from the subsurface ocean (Trumbo et al., 2019a, 2019b, 2022).

Fossae (Figure 1e) are long, narrow, depressions. The term is used for topographic features that occur on extraterrestrial planetary surfaces, whose exact origin is uncertain, although they are thought to be the result of predominantly extensional tectonic processes (Schenk et al., 2020). Considering their morphologies as troughs not exhibiting raised rims along their flanks, fossae represent the most primitive (in terms of fracture development) and commonly youngest type of fractures on Europa's surface (Kattenhorn & Marshall, 2006).

Here we investigate the region around Ménec Fossae on Europa (centered at 51°S, 177°W; on Europa's trailing hemisphere) for which we produced high-resolution photoclinometrically derived (Lesage et al., 2021; Schenk & Pappalardo, 2004) digital terrain models (DTMs) and a geomorphological-structural map (nominal scale 1:80,000). This area is of particular interest as it displays the interaction between bands, double ridges, chaotic terrains, and fossae, which might share common formation processes potentially related to refreezing, pressurization, and fracturing of shallow water reservoirs (Culberg et al., 2022).

Our results suggest that this area of Europa has undergone transtensional (strike-slip with a major extensional component) tectonic activity, as indicated by the orientation and relationship of the tectonic features present. Likely, such transtensional tectonism occurred above or associated with, shallow subsurface water, consistent with the presence of chaotic terrains and double ridges in the study area. Such a tectonic setting has possibly created a pathway facilitating the ascent of subsurface material, especially volatiles (Aydin, 2006; Greenberg et al., 2002).

2. Data and Methods

DTMs of the selected areas have been produced using the photoclinometry (PC) technique (e.g., Schenk & Pappalardo, 2004), through the Ames Stereo Pipeline (ASP, Beyer et al., 2018) Shape-from-Shading (SfS) tool (Alexandrov & Beyer, 2018). DTMs were derived from *Galileo*'s Solid-State Imager (SSI) images (Belton et al., 1992), which were processed through the Integrated Software for Imagers and Spectrometers (ISIS 4.4.0, https://isis.astrogeology.usgs.gov/7.0.0/index.html). In the final map, photogrammetrically controlled image mosaics were used as background (Bland, Weller, et al., 2021). For the processing of *Galileo* SSI raw image data, we used the SPICE smithed kernels (Bland, Weller, et al., 2021) and projected the processed data on a spheroid with a radius of 1560.800 km (i.e., the IAU-defined mean radius for Europa), which is therefore also the DTMs' reference height (Bland, Kirk, et al., 2021).

The PC/SfS technique overcomes the lack, on Europa, of having the same surface area covered by two or more images for traditional stereophotogrammetry DTMs' production. The smoothness parameter μ of the SfS tool, which weighs the smoothness of the resulting DTM and depends on surface properties, plays an important role and can vary the results significantly: optimal μ values with a good S/N ratio of the resulting DTM need to be found by trial and error, where different values need to be applied for each image (a detailed description of how μ affects the DTMs results can be found in Lesage et al., 2021). Manual quality checks have been conducted through features' height H estimations based on shadow lengths L and solar elevation angles α: H = Ltan(α). The SfS tool assumes uniformity in albedo and photometric parameters across the whole image, based on the reflectance model used. Here we have chosen the Hapke reflectance model, which is the most commonly adopted for icy moons (Belgacem et al., 2020). Even though such properties can change at regional or local scales, the overall uncertainties on the SfS DTMs vertical resolution are likely not more than 10%–15%, as previously discussed in the literature (Bierhaus & Schenk, 2010; Bland, Kirk, et al., 2021; Lesage et al., 2021; Schenk et al., 2020; Schenk & Pappalardo, 2004). We further conducted geomorphological-structural mapping of the selected areas on SSI images 9926r and 9939r in stereographic projection (image frames resolution of ~40 m/pixel, which corresponds to a nominal map scale of 1:80000) using QGIS3 (QGIS.org, 2022. QGIS Geographic Information System. QGIS Association. http://www.qgis.org) and the Mappy plugin (https://zenodo.org/record/5524389), units were distinguished based on morphology and albedo differences. Tectonic linear features such as faults were identified based on distinctive morphologies such as scarps, paired with topographical analysis of the DTMs.

3. Results

Ménec Fossae is located in the southern trailing hemisphere of Europa, near Thera and Thrace Maculae (Figure 2). We produced high-resolution DTMs of the study area (Figure 3), through the SfS technique described in Section 2.

We further conducted geomorphological analysis paired with fault mapping, resulting in a geomorphological-structural map of the Ménec Fossae area at a nominal scale of 1:80000 (Figure 4). We could distinguish six different geomorphological units (Chaotic Terrain, Double Ridge, Fossa, Crater, Ridged Plains, and Smooth Band), which are hereafter described and interpreted.
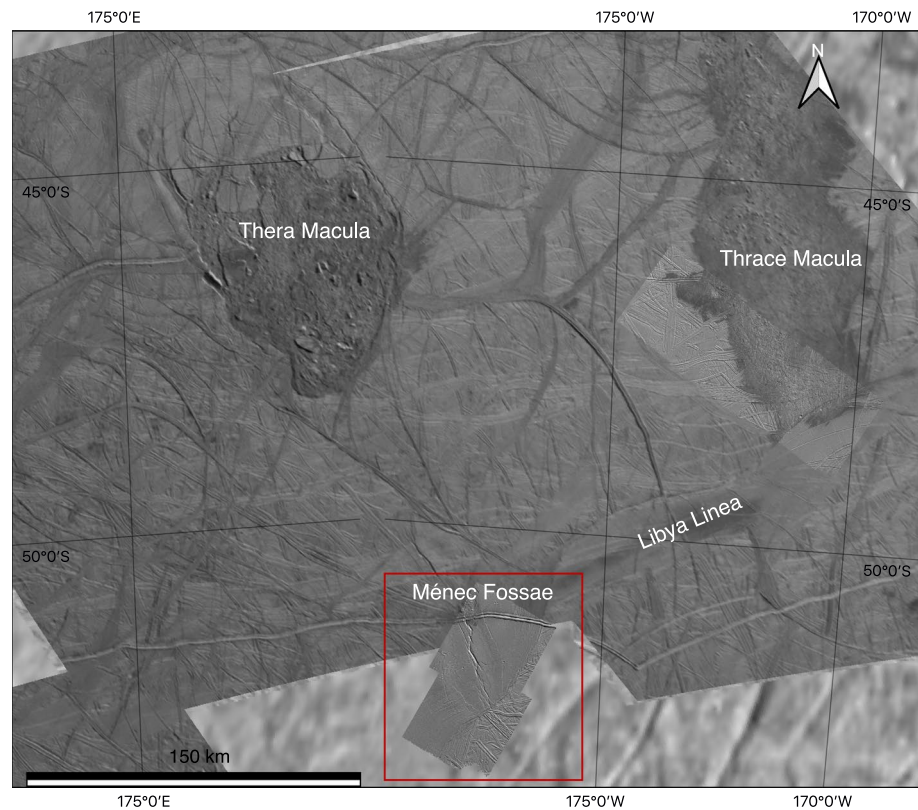
Figure 2. Regional map on photogrammetrically controlled *Galileo* Solid-State Imager image mosaics, the red box depicts the study area. To the NW, Thera Macula is recognizable, while Thrace Macula is located to the NE. Libya Linea, a large-scale smooth band, continues along from the NE-SW into Ménec Fossae.

3.1. Description and Interpretation of Geomorphological Units

3.1.1. Ridged Plains Unit

The Ridged Plains Unit (RPU) is characterized by a series of small-scale (∼200–500 m in width) high-albedo ridges which can be anywhere from sub-parallel to overlapping, in several cases in multiple orientations (Figure 4). In general, on Europa's surface, ridged plains are one of the oldest terrain types (Figueredo & Greeley, 2004; Greeley et al., 2000; Leonard et al., 2020; Pappalardo et al., 1999; Prockter et al., 1999). This is the case in the mapped area as well, as RPU's features are crosscut by all the units they are in contact with.

3.1.2. Smooth Band Unit

The Smooth Band Unit (SBU) consists of either very subdued ridges and troughs or material with little or no structure. In the mapped area (Figure 4), the SBU is a portion of the very large structure Libya Linea, which extends over thousands of km (Figure 2). Smooth bands are interpreted as regions of crustal extension in which the low relief and lack of internal structure can be due to small-scale fracturing or the emplacement of infilling material (e.g., Prockter et al., 2002).

3.1.3. Double Ridge Unit

The Double Ridge Unit (DRU) consists of two subparallel quasi-linear and symmetric topographically high landforms of relatively high albedo. The landforms are rounded to triangular in cross-section and separated by a trough that contains lower albedo material. In the northwestern part of the map (around 51.3°S, 177.8°W; Figure 4), the DRU has been incorporated into the Chaotic Terrain Unit (CTU), with a resulting topographic drop in the corresponding area, and therefore predates this unit (Figures 3 and 5f). It is important to note that the mapped double ridge exhibits flexural bulges and flanking troughs along both of its sides (Figure 5e), characteristics previously described by Dombard et al. (2013) who suggested that those double ridges displaying them likely originate from shallow water bodies. Although, such flanking features could be also related to surface flexure in the absence of water given the surface loading exerted by the ridge itself (e.g., Billings & Kattenhorn, 2005; Hurford et al., 2005; see Section 4.1).

On the regional map (Figure 2), the DRU is part of a much longer double ridge that has some elements with angular cusps similar to a cycloid (Hoppa et al., 1999). Nevertheless, it must be taken into account that at the map scale and within the Ménec Fossae setting, this DRU patch has all the geomorphological characteristics of a Europan double ridge and therefore we consider it as such. Furthermore, in the literature, there is a shared consensus to consider cycloidal ridges (such as the one part of DRU in the mapped area) as most likely having the same formation process as double ridges (Culberg et al., 2022; Figueredo & Greeley, 2004; Greenberg & Sak, 2014; Hoppa et al., 1999; Johnston & Montési, 2014).

3.1.4. Chaotic Terrain Unit

The CTU is formed by high albedo blocks or polygons of pre-existing crustal material, tens of meters to 1–2 km in size, within a low albedo hummocky matrix (Greeley et al., 2000; Leonard et al., 2018) that, in the studied area (Figure 4), lie generally at the same or lower level than the surrounding units, with locally higher crustal blocks (Figure 3).

3.1.5. Fossa Unit

The Fossa Unit (FU) is formed by topographically low (Figure 3), quasi-linear, landforms (Figure 4). In the mapped area, these depressions have steep sides, v-shaped cross sections, and many exhibit terraces; the most prominent of such features reaches depths of up to ∼200 m. Since it crosscuts all other mapped units and therefore postdates them, the FU is interpreted as the youngest unit in this area. In terms of fracture development, considering their morphologies as troughs not exhibiting raised rims along their flanks, fossae represent the most primitive and commonly youngest type of fractures on Europa's surface (Kattenhorn & Marshall, 2006).

3.1.6. Crater Unit

The Crater Unit (CU) consists of moderately high albedo material comprising a crater's floor, wall, and raised rim (Figure 4). It is interpreted as material excavated and/or deposited during impact events. Given their clustered appearance and the lack of significant ejecta blanket deposits, craters in this area of Europa have previously been interpreted as being secondary, that is, craters formed by material ejected from large primary impact craters (Bierhaus et al., 2005; Bierhaus & Schenk, 2010; Singer et al., 2013).

3.2. Stratigraphic Sequence

Based on the crosscutting relationships among the different geomorphological units, we could determine the following sequence of events (numbered, in brackets):

- RPU is the oldest terrain (1), as it occurs in most regions of Europa (Leonard et al., 2020).
- SBU (2), that is, a portion of Libya Linea, superimposes the RPU.
- Subsequently, the DRU (3) has formed; in the north-western edge of the mapped area, this unit has been incorporated in the CTU (4), which therefore postdates it.
- Ultimately, the FU (5) crosscuts all the other units it is in contact with, including the CTU (Figure 4; around 51.3°S, 177.9°W), suggesting the younger age of the FU. Although, considering that such crosscutting occurs only over a limited area, the CTU and FU could have formed contemporaneously, at least partially. The CU (6) is located on top of all other units, while there is no patch of such unit in contact with the FU, thus the cratering events were older or at least concurrent to the FU formation.

Such a stratigraphic sequence follows the typical three-stage development on Europa: the initial formation of ridged plains, followed by band-like features, and ultimately the imposition of chaotic terrains (Leonard et al., 2020). Individual double ridges instead appear to be continually forming on Europa's surface, with frequent crosscutting indicating a significant number of formation cycles throughout the icy moon's history (e.g., Prockter & Patterson, 2009).

3.3. Regional Faulting

Different types of faults have been identified and mapped. Note that many other faults are located in the southeastern part of the mapped area, within the RPU (Figure 4). Considering that this is the oldest of the mapped units, its complex and intense faulting suggests longer exposure to tectonic events and thus possibly to older tectonics, including events likely preceding those observed in the rest of the mapped area. Therefore, we did not distinguish them in the map and consider them as being part of the RPU's general rugged appearance.
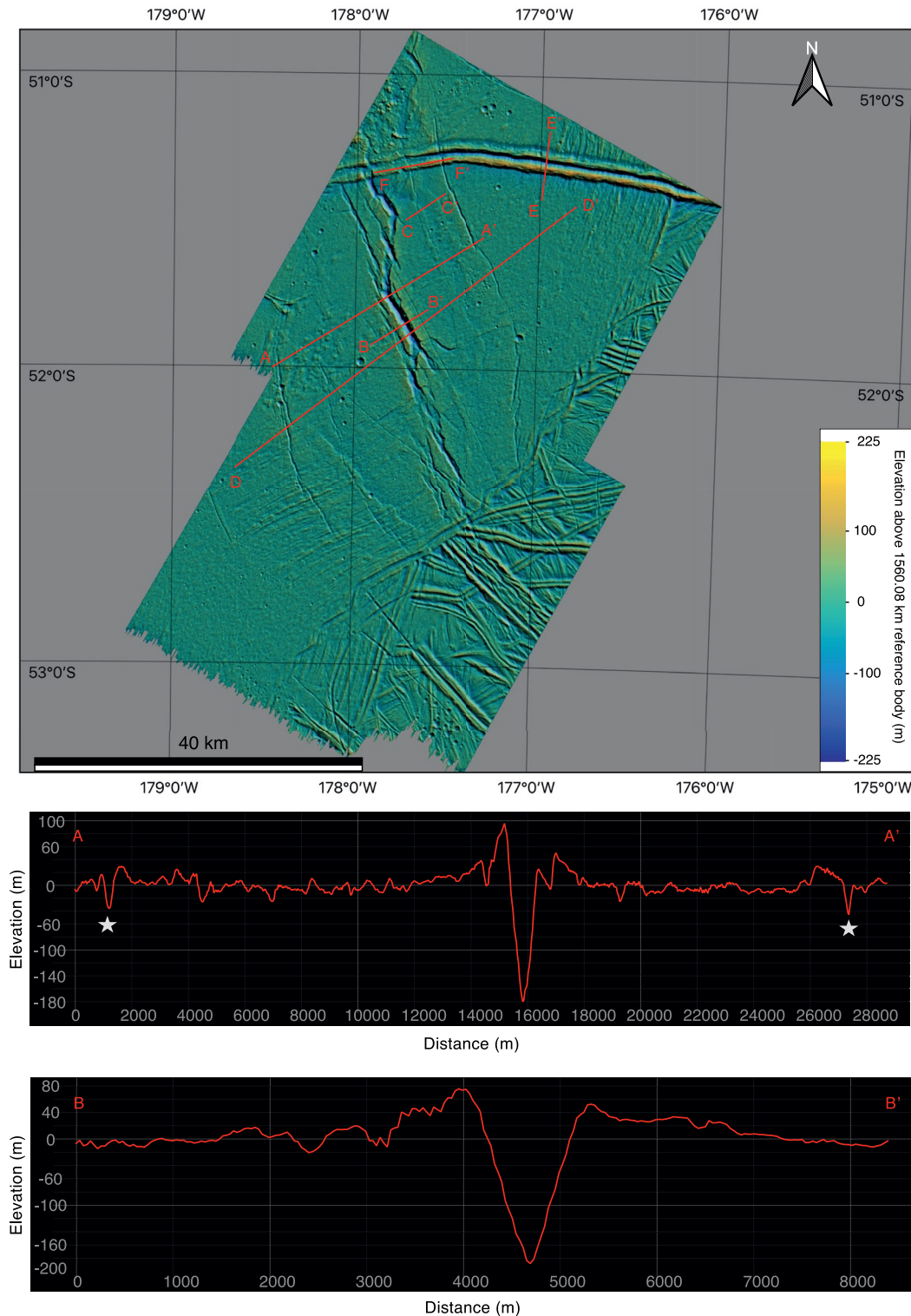
Figure 3. (top) Regional digital terrain model (DTM) of Ménec Fossae, individual DTMs are of 9926r and 9939r *Galileo* Solid-State Imager image frames, later mosaicked together. The DTM has smoothness parameter (μ) values of 0.004 for the southern 9926r image frame and 0.1 for the northern 9939r image frame. Image centered at 52°S, 177°W. Several elevation profile paths are shown, A-A′ and B-B′ profiles are displayed in the bottom panel (vertical exaggeration factor 1), and the others are displayed in Figure 5. (bottom) Elevation profiles. The main central depression reaches depths of ~200 m and is ~1 km wide along the elevation profile (detail in B-B′), with slope angle values of ~20–25° on the gentler southern side and of ~30–35° on the steeper northern side. Several minor depressions, flanking the main one, reach depths of 40–50 m (examples as star symbols in profile A-A′).
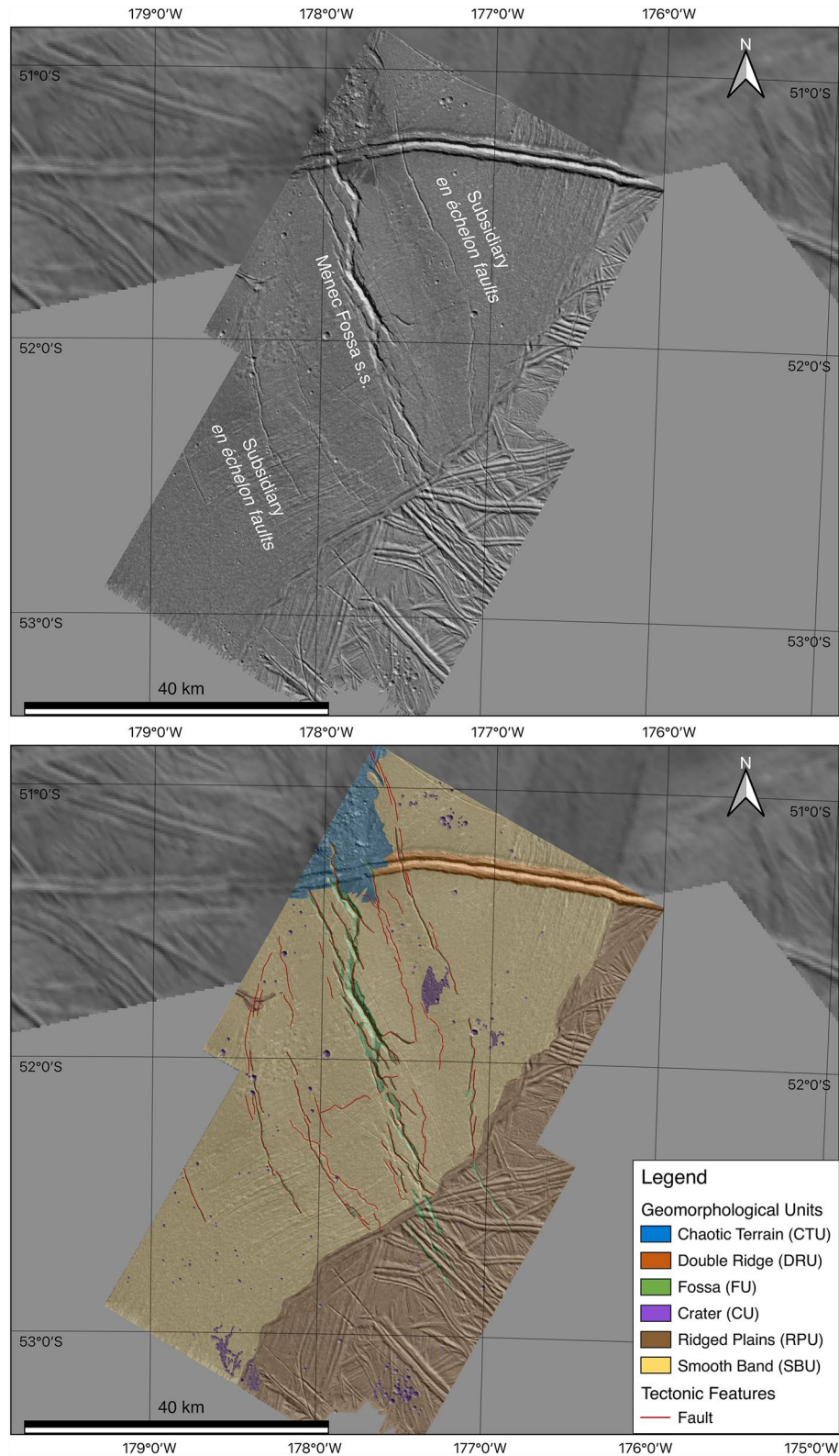
Figure 4. (top) Image mosaic of *Galileo* Solid-State Imager (SSI) 9926r and 9939r frames centered at 52°S, 177°W, displaying the area of Ménec Fossae. Photogrammetrically controlled SSI image mosaics as background. (bottom) Geomorphological-structural map of Ménec Fossae. A detailed interpretation of the tectonic features is given in the text (Section 4).
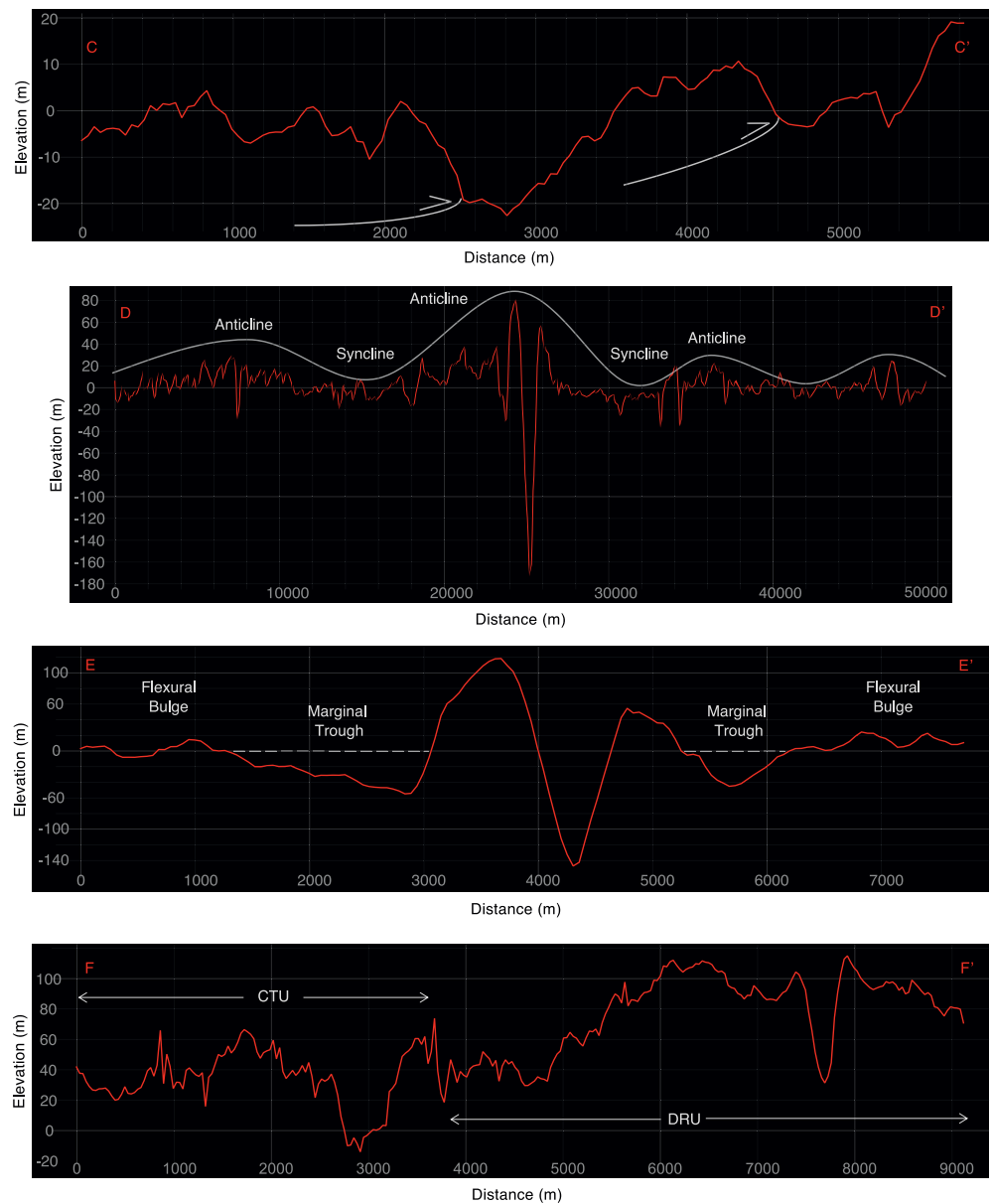
Figure 5. Elevation profiles along the digital terrain model at various locations, profiles' paths are displayed in Figure 3. (C-C′) Examples of mapped thrust faults, with hypothetical fault traces sketched in white. The two thrusts seem to follow a typical imbricate fan geometry. (D-D′) Long distance profile displaying the long-wavelength fold system discussed in Section 3.3. (E-E′) Detail of the double ridge (Double Ridge Unit (DRU)), depicting the observed marginal troughs and flexural bulges that likely support the shallow water reservoir hypothesis as its origin (Sections 3.1.3, 4, and 4.1). (F-F′) Detail of the CTU-DRU transition, showing the elevation drop corresponding to the incorporation of the DRU in the Chaotic Terrain Unit, proving the DRU relative older formation timing (Section 3.2).

Most of the mapped faults display both extensional and strike-slip characteristics, such as clear distinctive elevation drops yet with very steep sides and no clear hangingwall - footwall distinction (uncommon in purely extensional faults), along with *en échelon* disposition (Figures 3 and 4). Therefore, we consider them as transtensional faults (i.e., strike-slip features with an extensional component). The more prominent ones in terms of topographic drop have been mapped as part of the FU (Figure 4). These faults follow a roughly NW-SE trend and are distributed within three zones: around the center of the mapped area, Ménec Fossa *sensu stricto (s.s.*; from 51.3°S, 177.9°W to 52.5°S, 177.4°W; Figure 4) takes part most of the extensional component, spread along several quasi-parallel *en échelon* troughs, which become anastomosing toward their SE tips, reaching depths of up to ~200 m (Figure 3). These features are located along the anticline crest of a long-wavelength fold system, as previously observed in SSI image data (Prockter & Pappalardo, 2000) and further confirmed in this study through the newly available topographic information obtained from the DTM

(Figure 5d). On both sides of Ménec Fossa *s.s*, at distances of up to 10–15 km, two other sets of subsidiary *en échelon* transtensional faults subparallel to the main central features have been identified, aligned along NW-SE trends as well (from 50.8°S, 177.7°W to 51.9°S, 178.4°W and from 51.9°S, 178.4°W to 52.6°S, 178.2°W; Figure 4). These subsidiary faults have elevation drops of ~40–50 m in their deepest portions (Figure 3). Together with Ménec Fossa *s.s.* and the two sets of subsidiary flanking faults, other linear structures with lobate planform geometries have been identified (around 51.4°S, 177.7°W; 51.8°S, 177.3°W; 52.4°S, 177.9°W; Figure 4). These are flanking Ménec Fossa *s.s.* on both sides as well, with similar orientations. By tracing elevation profiles along the DTM, on an axis perpendicular to such linear structures (Figure 5c), it is possible to observe a clear increase in elevation followed by asymmetrical scarps. These characteristics are typical of compressive faults (Prockter & Pappalardo, 2000) on Earth and other planetary bodies (e.g., Mars, Titan) and we thus consider such linear structures as compressive tectonic features (i.e., thrust faults, Figures 5c and 6).

It is possible to note that the general fracturing pattern of the FU is non-uniform, there are at least two locations where this is most evident: centered at 51.4°S, 177.7°W, and 52.8°S, 177.6° (Figures 4 and 6), these two features
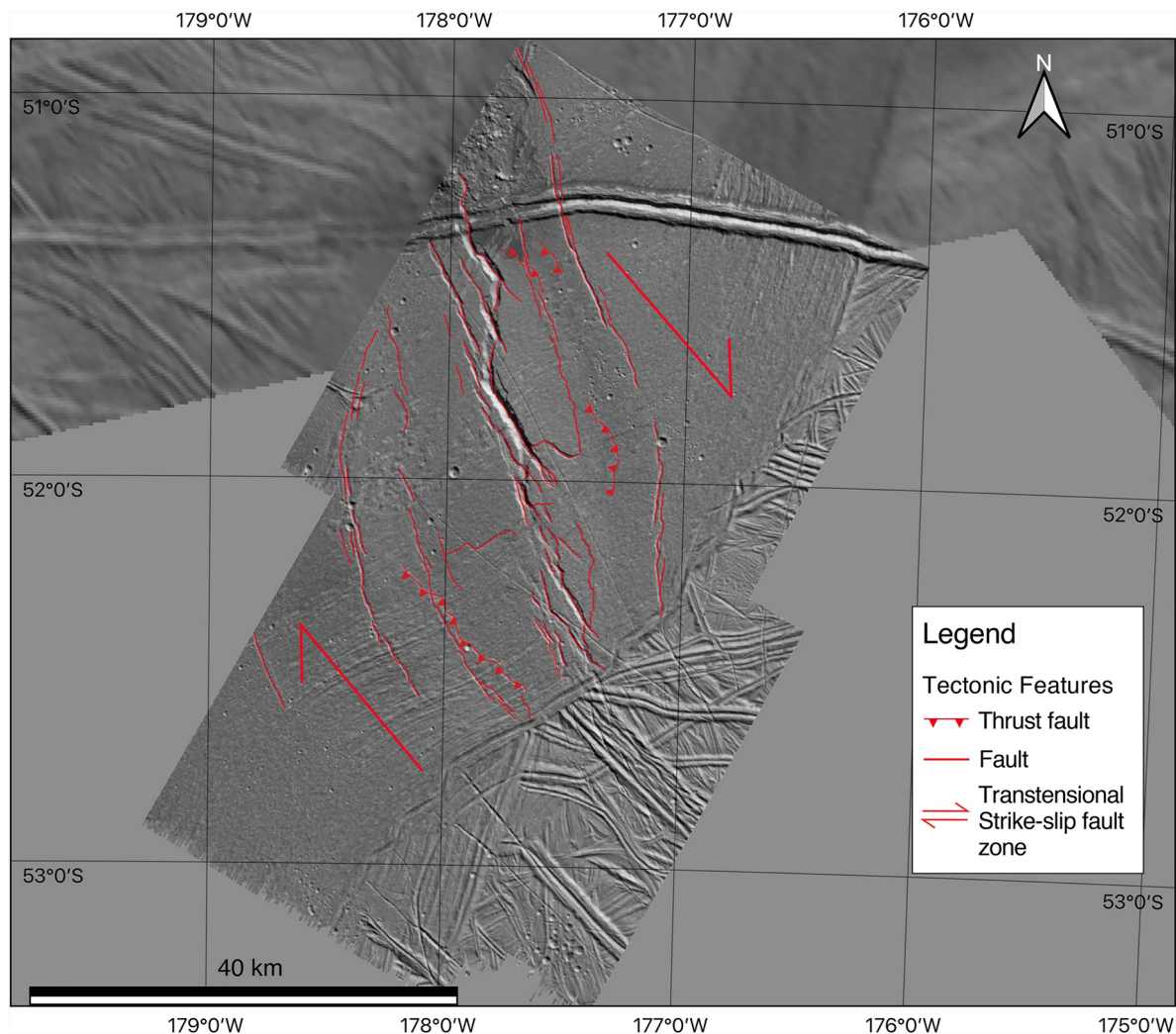

Figure 6. Proposed structural setting in the area of Ménec Fossae, image centered at 52°S, 177°W. The right-lateral strike-slip faulting controls the deformation along a wide shear zone, generating several extensional and transtensional features (marked together in the legend for ease of use of the structural map) and few compressive structures, in a predominantly transtensional (right-lateral) tectonic setting. An extensional component is thus present, yet limited with respect to the strike-slip one: by calculating a ~40° angle between the shear zone and the internal fractures' direction (Rossi et al., 2018), it is possible to quantitatively determine the amount of extension within the shear zone as being ~10%. Local portions have a larger compressional component, resulting in folding (see Figure 5d) and thrust faulting (Figure 5c). Furthermore, secondary cracks are locally present, evidence of non-uniform fracturing (see Section 3.3).

are located in the proximity of faults' tips and have different orientations from the main local trend of NW-SE, the former along an ESE-WNW trend and the latter is curved but it is oriented roughly E-W. We interpret these two features as secondary fractures, not primarily caused by global tidal stresses, but instead resulting from lateral motion along strike-slip faults (Kattenhorn, 2004).

4. Discussion

Several formation hypotheses have been previously proposed for the area of Ménec Fossae. Prockter and Pappalardo (2000) consider it as a regional scale anticline (upward convex) fold's crest flanked by small reverse faults, which are inferred to mark syncline (upward concave) folds' hinges. In this case, the folding and associated small-scale thrust faulting would imply that compression was, or is, ongoing in this area of Europa, which would locally compensate for the ubiquitous extension observed on the surface of this Jupiter's icy moon. More recently, it has been suggested (Schenk et al., 2020) that Ménec Fossa is part of a set of *en échelon* fissures associated with True Polar Wander (TPW) of the ice shell (Schenk et al., 2008), involving a 70° global rotation of surface features. The authors consider these features as sets of multiple parallel faults in which most of the extension is confined within a single narrow central feature. The fissures are also thought to be closely associated with buckling or tilting of the surface by a few tens of meters within the deformation zone. Other features on Europa associated with TPW (Schenk et al., 2020) include the same terrain type, displaying similar geomorphological and structural characteristics as Ménec Fossae (Kermario Fossae—43°N, 5°E (Figure 1e); Kerlescan Fossae—3°N, 238°W).

Based on geomorphological and topographical observations of the Ménec Fossae area, our hypothesis for its formation mechanisms involves transtensional tectonics (Figure 6) likely above, or associated with a shallow water reservoir. Such a hypothesis considers the two main previous models on this area, described above (Prockter & Pappalardo, 2000; Schenk et al., 2020), together with proposed mechanisms for the formation of different surface features on Europa, including chaotic terrains and double ridges (e.g., Chivers et al., 2021; Craft et al., 2016; Culberg et al., 2022; Dombard et al., 2013; Kalousová et al., 2016; B. E. Schmidt et al., 2011), which are present in the study area. These last contributions all invoke the emplacement of shallow water bodies within the ice shell to generate the various surface expressions they focus on. In particular, by comparison with an analysis of a terrestrial double ridge in Greenland, Culberg et al. (2022) show how double ridges might form via refreezing, pressurization, and fracturing of shallow water reservoirs, potentially induced by shear heating (Han & Showman, 2008; Kalousová et al., 2016; Nimmo & Gaidos, 2002). Dombard et al. (2013) suggest as well that shallow water reservoirs must be involved in double ridge formation in order to explain the aforementioned flanking features, where those are present. However, this kind of flanking topography can also be accommodated by surface flexure in the absence of water, given the surface loading exerted by the double ridge itself (e.g., Billings & Kattenhorn, 2005; Hurford et al., 2005). Nevertheless, Dombard et al. (2013) concluded that, among the potential formation mechanisms for double ridges, only a shallow water body ∼1–2 km beneath the feature could provide a thermal anomaly sufficient to account for the observation of flanking features (Craft et al., 2016). These processes may also operate in conjunction with other proposed double ridges formation mechanisms, such as shear heating (Johnston & Montési, 2014).

In this study, through analyses of the geomorphological units and tectonic features of the Ménec Fossae area, located within the smooth band Libya Linea, we identify a deep central feature (Ménec Fossa s.s.; Figures 4 and 6) that takes up most of the extension, flanked by numerous quasi-parallel subsidiary extensional and strike-slip faults and few thrust faults, all in a deformation zone 20–30 km wide (see Section 3.3). We propose that such a tectonic setting is generated within a right-lateral strike-slip fault zone, with a ∼10% contribution by an extensional component (Rossi et al., 2018), that is, a transtensional tectonic setting (Figure 6). Transtensional features are widespread on Earth, mainly within large-scale strike-slip settings (Donzé et al., 2021). They have also been observed on terrestrial planets (e.g., Mars, Andrews-Hanna et al., 2008; G. Schmidt et al., 2022) and other ocean worlds, Ganymede (e.g., Rossi et al., 2018), Enceladus (e.g., Rossi et al., 2020), and Titan (e.g., Burkhard et al., 2022; Matteoni et al., 2020). Several other examples exist on Europa as well, such as along Agenor Linea in the southern trailing hemisphere and Astypalaea Linea in the south polar region (Hoyer et al., 2014; Prockter et al., 2000; Tufts et al., 1999, 2000). In transtensional tectonic regimes, minor compressional features are common and expected (Fossen et al., 1994; Petit, 1987). In this context, the small thrust faults observed (around 51.4°S, 177.7°W; 51.8°S, 177.3°W; 52.4°S, 177.9°W; Figure 6) are consistent as being formed within a

predominantly transtensional setting. This hypothesis does not rule out that of Prockter and Pappalardo (2000), which consider such thrust faults as marking synclinal folds' hinges and Ménec Fossa s.s. as a regional scale anticline's crest within the same fold system. Folding in transtensional settings (on an oblique axis with respect to the major strike-slip fault zone, as we observe in the study area) is, in fact, also common (Fossen et al., 1994).

Fault motions on Europa have been hypothesized to be driven by diurnal tidal stresses (Greenberg et al., 1998), which rotate in a relatively opposite sense in the north and south hemispheres. This cycle, referred to as tidal walking (Hoppa, 1999), predicts the sense of offset along strike-slip faults in the context of global tidal stresses. The overall result is that strike-slip faults accumulate displacements over time, with a preponderance of left-lateral offsets in the northern hemisphere and right-lateral offsets in the southern hemisphere (with variations dependent on fault orientation within 30° of the equator), in agreement with observed offset. along large faults (Hoppa, 1999; Sarid, 2002). However, this model is not necessarily compatible with all fault slip sense characteristics on Europa (Kattenhorn, 2004); it does not account for the whole range of fault morphologies, nor does it consider fault slip behavior and related deformation such as secondary fracturing (e.g., tailcracks and anti-cracks, Kattenhorn & Marshall, 2006). In response to the shear motion, the perturbed stress field at the tip of the fault is in fact both greater in magnitude and different in principal stress orientations to the remote (far-field) stress that caused the fault to slip. Thus, perturbed stress fields are likely the driving mechanism for the development of secondary fractures, such as tailcracks in regions of high tension (extensional quadrants), and anti-cracks in - mutually opposite to the tensional ones - regions of increased compression (compressive quadrants) at the fault tip (Kattenhorn, 2004; Kattenhorn & Marshall, 2006).

In the Ménec Fossae area, our analyses are consistent with what is discussed above, as we observe a right-lateral strike-slip fault system with a 10% transtensional component (Rossi et al., 2018) in the trailing southern hemisphere of Europa, displaying evidence of non-uniform cracking such as secondary fractures resulting from lateral motion along strike-slip faults (Kattenhorn, 2004; Kattenhorn & Marshall, 2006). Considering that such a tectonic setting developed within the smooth band Libya Linea, we reckon that the band's dynamics, likely related to the daily rotation of the diurnal tidal stresses (Kattenhorn, 2004), are the primary driving mechanisms for the observed tectonic pattern and associated fracturing. Furthermore, the morphological characteristics of the FU match with those of troughs (Figure 4), considered the most primitive (in terms of fracture development) and youngest type of fracture (see Sections 1 and 3.1.5). The FU formed within the band Libya Linea, with bands, in comparison to troughs, representing the opposite end-member in an evolutionary sequence of fracture development (Kattenhorn & Marshall, 2006). Thus, the presence of the FU likely indicates the beginning of a novel and distinct fracturing pattern within Libya Linea. This observation suggests a relatively young formation and development age for the FU, whose associated fault system has possibly created a pathway facilitating the ascent of subsurface material (Aydin, 2006; Greenberg et al., 2002). Compositional information is not available for the study area as there are no *Galileo* Near Infrared Mapping Spectrometer (NIMS) data at this location. Such information would have been essential for the detailed characterization of fresh subsurface material potentially emplaced by the Ménec Fossae fault system.

4.1. Implications for Shallow Subsurface Water and Other Scenarios

The setting at Ménec Fossae that is presented here could be related to several mechanisms, including, among others, diapirism (e.g., Head & Pappalardo, 1999), lithosphere bending and folding (e.g., Prockter & Pappalardo, 2000), TPW (Schenk et al., 2020), and emplacement of a water body located at shallow depths within the ice shell (e.g., Dombard et al., 2013; B. E. Schmidt et al., 2011). The first two hypotheses might be concomitant and could both explain the observed long-wavelength topography (Figure 5d) and the extensional troughs at anticlines' crests (see Section 4), while the local faulting pattern is in agreement with the TPW hypothesis. Nonetheless, we reckon that the described transtensional tectonic setting most likely occurred above or associated with a shallow water reservoir, consistently with the presence of the CTU and DRU to the north of Ménec Fossa s.s. (Figure 4, Chivers et al., 2021; Craft et al., 2016; Culberg et al., 2022; Dombard et al., 2013; Kalousová et al., 2016; B. E. Schmidt et al., 2011). In fact, the shallow water body hypothesis is strongly supported by the overall lower elevation of the CTU compared to its surroundings (Figure 5f), considering that liquid water beneath chaos should have this kind of topographic expression on the surface, as it seems to occur at the nearby feature Thera Macula (B. E. Schmidt et al., 2011). The presence of the flexural bulges and flanking troughs (Figure 5e) on both sides of the DRU (Craft et al., 2016; Dombard et al., 2013) further strengthens the case, as discussed in Sections 3.1.3 and 4.

The long-wavelength topography observed (Figure 5d) supports this hypothesis as well, matching the expected surface expression above shallow water bodies at a late development stage (Manga & Michaut, 2017). Therefore, we consider the shallow water body hypothesis as the most consistent with the overall morphology and topography of the Ménec Fossae area. The majority of formation models for the emplacement of shallow water reservoirs have determined depths of 1–5 km beneath various geological features (lenticulae, chaos, double ridges, Chivers et al., 2021; Craft et al., 2016; Dombard et al., 2013; Johnston & Montési, 2014; Kalousová et al., 2016; Manga & Michaut, 2017; B. E. Schmidt et al., 2011), with estimates varying depending on the adopted thickness of Europa's ice shell. We thus assume a hypothetical water reservoir's emplacement depth within such range in the study area, in agreement with the observed lowest elevations at Ménec Fossae of $\sim$−200 m (see Section 3.3).

5. Conclusions

We conclude that the area of Ménec Fossae has been shaped by transtensional tectonic activity, likely above, or associated with a water reservoir located at shallow depths within Europa's ice shell. Ménec Fossae is situated within the large-scale smooth band Libya Linea, indicating that the dynamics of the band are likely the primary driving mechanisms for the observed transtensional tectonic setting. The ascent of subsurface material along the Ménec Fossae fault system is plausible, particularly when considering the proposed shallow water reservoir hypothesis. These results, together with ongoing work on other areas of Europa's surface, contribute to identifying the most probable regions to find fresh material, representative of the subsurface ocean. Furthermore, they will serve as input data for dust ejecta trajectory models, ultimately supporting the compositional mapping of Europa's surface by the time-of-flight mass spectrometer Surface Dust Analyzer (SUDA), onboard the upcoming *Europa Clipper* mission (Goode et al., 2021, 2023; Kempf et al., 2014; Postberg et al., 2011). The model presented here provides a possible explanation for the formation of an intriguing area of Europa that exhibits several major terrain types, while also strengthening the case for the existence of widely distributed shallow water reservoirs within Europa's ice shell.

Data Availability Statement

Galileo's SSI data used in this manuscript can be accessed from the PDS Cartography and Imaging Science Node (Thaller, 2000), while the SSI photogrammetrically corrected base map mosaics can be accessed from the USGS Astrogeology website (Bland & Lynn, 2021). The Digital Terrain Model (Figure 3) and data from the geomorphological-structural map (Figure 4) produced are available on TRR 170-DB (Matteoni, 2022).

References

Alexandrov, O., & Beyer, R. A. (2018). Multiview shape-from-shading for planetary images. *Earth and Space Science*, *5*(10), 652–666. https://doi.org/10.1029/2018EA000390

Anderson, J. D., Schubert, G., Jacobson, R. A., Lau, E. L., Moore, W. B., & Sjogren, W. L. (1998). Europa's differentiated internal structure: Inferences from four Galileo encounters. *Science*, *281*(5385), 2019–2022. https://doi.org/10.1126/science.281.5385.2019

Andrews-Hanna, J. C., Zuber, M. T., & Hauck, S. A. (2008). Strike-slip faults on Mars: Observations and implications for global tectonics and geodynamics. *Journal of Geophysical Research*, *113*(E8), E08002. https://doi.org/10.1029/2007JE002980

Aydin, A. (2006). Failure modes of the lineaments on Jupiter's moon, Europa: Implications for the evolution of its icy crust. *Journal of Structural Geology*, *28*(12), 2222–2236. https://doi.org/10.1016/j.jsg.2006.08.003

Barr, A. C., & Pappalardo, R. T. (2005). Onset of convection in the icy Galilean satellites: Influence of rheology. *Journal of Geophysical Research*, *110*(E12), E12005. https://doi.org/10.1029/2004JE002371

Běhounková, M., Tobie, G., Choblet, G., Kervazo, M., Melwani Daswani, M., Dumoulin, C., & Vance, S. D. (2021). Tidally induced magmatic pulses on the oceanic floor of Jupiter's Moon Europa. *Geophysical Research Letters*, *48*(3), 1–11. https://doi.org/10.1029/2020GL090077

Belgacem, I., Schmidt, F., & Jonniaux, G. (2020). Regional study of Europa's photometry. *Icarus*, *338*, 113525. https://doi.org/10.1016/j.icarus.2019.113525

Belton, M. J. S., Klaasen, K. P., Clary, M. C., Anderson, J. L., Anger, C. D., Carr, M. H., et al. (1992). The Galileo solid-state imaging experiment. *Space Science Reviews*, *60*(1–4), 413–455. https://doi.org/10.1007/BF00216864

Beyer, R. A., Alexandrov, O., & McMichael, S. (2018). The Ames stereo pipeline: NASA's open source software for deriving and processing terrain data. *Earth and Space Science*, *5*(9), 537–548. https://doi.org/10.1029/2018EA000409

Bierhaus, E. B., Chapman, C. R., & Merline, W. J. (2005). Secondary craters on Europa and implications for cratered surfaces. *Nature*, *437*(7062), 1125–1127. https://doi.org/10.1038/nature04069

Bierhaus, E. B., & Schenk, P. M. (2010). Constraints on Europa's surface properties from primary and secondary crater morphology. *Journal of Geophysical Research: Planets*, *115*(12), 1–17. https://doi.org/10.1029/2009JE003451

Bierhaus, E. B., Zahnle, K., & Chapman, C. R. (2009). Europa's crater distributions and surface ages. In *Europa* (pp. 161–180). University of Arizona Press. https://doi.org/10.2307/j.ctt1xp3wdw.13

Billings, S. E., & Kattenhorn, S. A. (2005). The great thickness debate: Ice shell thickness models for Europa and comparisons with estimates based on flexure at ridges. *Icarus*, *177*(2), 397–412. https://doi.org/10.1016/j.icarus.2005.03.013

Bland, M., & Lynn, W. (2021). Photogrammetrically controlled equirectangular Galileo image mosaics of Europa. [Dataset]. U.S. Geological Survey. https://doi.org/10.5066/P9VKKK7C

Bland, M. T., Kirk, R. L., Galuszka, D. M., Mayer, D. P., Beyer, R. A., & Fergason, R. L. (2021). How well do we know Europa's topography? An evaluation of the variability in digital terrain models of Europa. *Remote Sensing*, *13*(24), 5097. https://doi.org/10.3390/rs13245097

Bland, M. T., Weller, L. A., Archinal, B. A., Smith, E., & Wheeler, B. H. (2021). Improving the usability of Galileo and voyager images of Jupiter's Moon Europa. *Earth and Space Science*, *8*(12). https://doi.org/10.1029/2021EA001935

Buffo, J. J., Schmidt, B. E., Huber, C., & Walker, C. C. (2020). Entrainment and dynamics of ocean-derived impurities within Europa's Ice Shell. *Journal of Geophysical Research: Planets*, *125*(10), 1–23. https://doi.org/10.1029/2020JE006394

Burkhard, L. M. L., Smith-Konter, B. R., Fagents, S. A., Cameron, M. E., Collins, G. C., & Pappalardo, R. T. (2022). Strike-slip faulting on Titan: Modeling tidal stresses and shear failure conditions due to pore fluid interactions. *Icarus*, *371*, 114700. https://doi.org/10.1016/j.icarus.2021.114700

Carr, M. H., Belton, M. J. S., Chapman, C. R., Davies, M. E., Geissler, P., Greenberg, R., et al. (1998). Evidence for a subsurface ocean on Europa. *Nature*, *391*(6665), 363–365. https://doi.org/10.1038/34857

Chivers, C. J., Buffo, J. J., & Schmidt, B. E. (2021). Thermal and chemical evolution of small, shallow water bodies in Europa's ice shell. *Journal of Geophysical Research: Planets*, *126*(5), 1–26. https://doi.org/10.1029/2020JE006692

Collins, G., & Nimmo, F. (2009). Chaotic terrain on Europa. In *Europa* (pp. 259–282). University of Arizona Press. https://doi.org/10.2307/j.ctt1xp3wdw.17

Craft, K. L., Patterson, G. W., Lowell, R. P., & Germanovich, L. (2016). Fracturing and flow: Investigations on the formation of shallow water sills on Europa. *Icarus*, *274*, 297–313. https://doi.org/10.1016/j.icarus.2016.01.023

Culberg, R., Schroeder, D. M., & Steinbrügge, G. (2022). Double ridge formation over shallow water sills on Jupiter's moon Europa. *Nature Communications*, *13*(1), 1–10. https://doi.org/10.1038/s41467-022-29458-3

Dalton, J. B., Prieto-Ballesteros, O., Kargel, J. S., Jamieson, C. S., Jolivet, J., & Quinn, R. (2005). Spectral comparison of heavily hydrated salts with disrupted terrains on Europa. *Icarus*, *177*(2), 472–490. https://doi.org/10.1016/j.icarus.2005.02.023

Dalton, J. B., Shirley, J. H., & Kamp, L. W. (2012). Europa's icy bright plains and dark linea: Exogenic and endogenic contributions to composition and surface properties. *Journal of Geophysical Research*, *117*(E3), E03003. https://doi.org/10.1029/2011JE003909

Dombard, A. J., Patterson, G. W., Lederer, A. P., & Prockter, L. M. (2013). Flanking fractures and the formation of double ridges on Europa. *Icarus*, *223*(1), 74–81. https://doi.org/10.1016/j.icarus.2012.11.021

Donzé, F.-V., Klinger, Y., Bonilla-Sierra, V., Duriez, J., Jiao, L., & Scholtès, L. (2021). Assessing the brittle crust thickness from strike-slip fault segments on Earth, Mars and Icy moons. *Tectonophysics*, *805*, 228779. https://doi.org/10.1016/j.tecto.2021.228779

Fagents, S. A. (2003). Considerations for effusive cryovolcanism on Europa: The post-Galileo perspective. *Journal of Geophysical Research*, *108*(E12), 13–21. https://doi.org/10.1029/2003JE002128

Figueredo, P. H., & Greeley, R. (2004). Resurfacing history of Europa from pole-to-pole geological mapping. *Icarus*, *167*(2), 287–312. https://doi.org/10.1016/j.icarus.2003.09.016

Fossen, H., Tikoff, B., & Teyssier, C. (1994). Strain modeling of transpressional and transtensional deformation. *Norsk Geologisk Tidsskrift*, *74*(3), 134–145.

Goode, W., Kempf, S., & Schmidt, J. (2021). Detecting the surface composition of geological features on Europa and Ganymede using a surface dust analyzer. *Planetary and Space Science*, *208*, 105343. https://doi.org/10.1016/j.pss.2021.105343

Goode, W., Kempf, S., & Schmidt, J. (2023). Mapping the surface composition of Europa with SUDA. *Planetary and Space Science*, *227*, 105633. https://doi.org/10.1016/j.pss.2023.105633

Greeley, R., Chyba, C. F., Head, I. I. I. J. W., McCord, T. B., McKinnon, W. B., Pappalardo, R. T., & Figueredo, P. H. (2004). Geology of Europa. Jupiter. The planet, satellites and magnetosphere.

Greeley, R., Figueredo, P. H., Williams, D. A., Chuang, F. C., Klemaszewski, J. E., Kadel, S. D., et al. (2000). Geologic mapping of Europa. *Journal of Geophysical Research*, *105*(E9), 22559–22578. https://doi.org/10.1029/1999JE001173

Greenberg, R., & Geissler, P. (2002). Europa's dynamic icy crust. *Meteoritics & Planetary Sciences*, *37*(12), 1685–1710. https://doi.org/10.1111/j.1945-5100.2002.tb01158.x

Greenberg, R., Geissler, P., Hoppa, G., & Tufts, B. R. (2002). Tidal-tectonic processes and their implications for the character of Europa's icy crust. *Reviews of Geophysics*, *40*(2), 1-1–1-33. https://doi.org/10.1029/2000RG000096

Greenberg, R., Geissler, P., Hoppa, G., Tufts, B. R., Durda, D. D., Pappalardo, R., et al. (1998). Tectonic processes on Europa: Tidal stresses, mechanical response, and visible features. *Icarus*, *135*(1), 64–78. https://doi.org/10.1006/icar.1998.5986

Greenberg, R., Geissler, P., Tufts, B. R., & Hoppa, G. V. (2000). Habitability of Europa's crust: The role of tidal-tectonic processes. *Journal of Geophysical Research*, *105*(E7), 17551–17562. https://doi.org/10.1029/1999JE001147

Greenberg, R., Hoppa, G. V., Bart, G., & Hurford, T. (2003). Tidal stress patterns on Europa's crust. *Celestial Mechanics and Dynamical Astronomy*, *87*(1–2), 171–188. https://doi.org/10.1023/A:1026169424511

Greenberg, R., & Sak, P. B. (2014). The ridges of Europa: Extensions of adjacent topography onto their flanks. *Earth and Planetary Science Letters*, *389*, 43–51. https://doi.org/10.1016/j.epsl.2013.12.009

Han, L., & Showman, A. P. (2008). Implications of shear heating and fracture zones for ridge formation on Europa. *Geophysical Research Letters*, *35*(3), L03202. https://doi.org/10.1029/2007GL031957

Hand, K. P., & Carlson, R. W. (2015). Europa's surface color suggests an ocean rich with sodium chloride. *Geophysical Research Letters*, *42*(9), 3174–3178. https://doi.org/10.1002/2015GL063559

Hand, K. P., Phillips, C. B., Murray, A., Garvin, J. B., Maize, E. H., Gibbs, R. G., et al. (2022). Science goals and mission architecture of the Europa lander mission concept. *The Planetary Science Journal*, *3*(1), 22. https://doi.org/10.3847/PSJ/ac4493

Hansen, G. B., & McCord, T. B. (2008). Widespread CO2 and other non-ice compounds on the anti-Jovian and trailing sides of Europa from Galileo/NIMS observations. *Geophysical Research Letters*, *35*(1), 2–6. https://doi.org/10.1029/2007GL031748

Head, J. W., & Pappalardo, R. T. (1999). Brine mobilization during lithospheric heating on Europa: Implications for formation of chaos terrain, lenticula texture, and color variations. *Journal of Geophysical Research*, *104*(E11), 27143–27155. https://doi.org/10.1029/1999JE001062

Hoppa, G. (1999). Strike–slip faults on Europa: Global shear patterns driven by tidal stress. *Icarus*, *141*(2), 287–298. https://doi.org/10.1006/icar.1999.6185

Hoppa, G. V., Tufts, B. R., Greenberg, R., & Geissler, P. E. (1999). Formation of cycloidal features on Europa. *Science*, *285*(5435), 1899–1902. https://doi.org/10.1126/science.285.5435.1899

Howell, S. M. (2021). The likely thickness of Europa's Icy Shell. *The Planetary Science Journal*, *2*(4), 129. https://doi.org/10.3847/PSJ/abfe10

Hoyer, L., Kattenhorn, S. A., & Watkeys, M. K. (2014). Multistage evolution and variable motion history of Agenor Linea, Europa. *Icarus*, *232*, 60–80. https://doi.org/10.1016/j.icarus.2013.12.010

Hurford, T. A., Beyer, R. A., Schmidt, B., Preblich, B., Sarid, A. R., & Greenberg, R. (2005). Flexure of Europa's lithosphere due to ridge-loading. *Icarus*, *177*(2), 380–396. https://doi.org/10.1016/j.icarus.2005.06.019

Hussmann, H. (2002). Thermal equilibrium states of Europa's Ice Shell: Implications for internal ocean thickness and surface heat flow. *Icarus*, *156*(1), 143–151. https://doi.org/10.1006/icar.2001.6776

Hussmann, H., Choblet, G., Lainey, V., Matson, D. L., Sotin, C., Tobie, G., & Van Hoolst, T. (2010). Implications of rotation, orbital states, energy sources, and heat transport for internal processes in icy satellites. *Space Science Reviews*, *153*(1–4), 317–348. https://doi.org/10.1007/s11214-010-9636-0

Johnston, S. A., & Montési, L. G. J. (2014). Formation of ridges on Europa above crystallizing water bodies inside the ice shell. *Icarus*, *237*, 190–201. https://doi.org/10.1016/j.icarus.2014.04.026

Kalousová, K., Souček, O., Tobie, G., Choblet, G., & Čadek, O. (2016). Water generation and transport below Europa's strike-slip faults. *Journal of Geophysical Research: Planets*, *121*(12), 2444–2462. https://doi.org/10.1002/2016JE005188

Kattenhorn, S. A. (2004). Strike-slip fault evolution on Europa: Evidence from tailcrack geometries. *Icarus*, *172*(2), 582–602. https://doi.org/10.1016/j.icarus.2004.07.005

Kattenhorn, S. A., & Hurford, T. (2009). Tectonics of Europa. In *Europa* (pp. 199–236). University of Arizona Press.

Kattenhorn, S. A., & Marshall, S. T. (2006). Fault-Induced perturbed stress fields and associated tensile and compressive deformation at fault tips in the ice shell of Europa: Implications for fault mechanics. *Journal of Structural Geology*, *28*(12), 2204–2221. https://doi.org/10.1016/j.jsg.2005.11.010

Kattenhorn, S. A., & Prockter, L. M. (2014). Evidence for subduction in the ice shell of Europa. *Nature Geoscience*, *7*(10), 762–767. https://doi.org/10.1038/ngeo2245

Kempf, S., Altobelli, N., Briois, C., Grün, E., Horanyi, M., Postberg, F., et al. (2014). SUDA: A dust mass spectrometer for compositional surface mapping for a mission to Europa. *European Planetary Science Congress*. Retrieved from http://adsabs.harvard.edu/abs/2014EPSC….9..229K

Khurana, K. K., Kivelson, M. G., Stevenson, D. J., Schubert, G., Russell, C. T., Walker, R. J., & Polanskey, C. (1998). Induced magnetic fields as evidence for subsurface oceans in Europa and Callisto. *Nature*, *395*(6704), 777–780. https://doi.org/10.1038/27394

Kivelson, M. G., Khurana, K. K., Russell, C. T., Volwerk, M., Walker, R. J., & Zimmer, C. (2000). Galileo magnetometer measurements: A stronger case for a subsurface ocean at Europa. *Science*, *289*(5483), 1340–1343. https://doi.org/10.1126/science.289.5483.1340

Leonard, E. J., Pappalardo, R. T., & Yin, A. (2018). Analysis of very-high-resolution Galileo images and implications for resurfacing mechanisms on Europa. *Icarus*, *312*, 100–120. https://doi.org/10.1016/j.icarus.2018.04.016

Leonard, E. J., Yin, A., & Pappalardo, R. T. (2020). Ridged plains on Europa reveal a compressive past. *Icarus*, *343*, 113709. https://doi.org/10.1016/j.icarus.2020.113709

Lesage, E., Schmidt, F., Andrieu, F., & Massol, H. (2021). Constraints on effusive cryovolcanic eruptions on Europa using topography obtained from Galileo images. *Icarus*, *361*, 114373. https://doi.org/10.1016/j.icarus.2021.114373

Ligier, N., Poulet, F., Carter, J., Brunetto, R., & Gourgeot, F. (2016). Vlt/Sinfoni observations of Europa: New insights into the surface composition. *The Astronomical Journal*, *151*(6), 163. https://doi.org/10.3847/0004-6256/151/6/163

Manga, M., & Michaut, C. (2017). Formation of lenticulae on Europa by saucer-shaped sills. *Icarus*, *286*, 261–269. https://doi.org/10.1016/j.icarus.2016.10.009

Matteoni, P. (2022). Replication data for: Ménec fossae on Europa: A strike-slip tectonics origin above a possible shallow water reservoir. [Dataset]. TRR170-DB, V1. https://doi.org/10.35003/8CU23S

Matteoni, P., Mitri, G., Poggiali, V., & Mastrogiuseppe, M. (2020). Geomorphological analysis of the southwestern margin of Xanadu, Titan: Insights on tectonics. *Journal of Geophysical Research: Planets*, *125*(12), 1–22. https://doi.org/10.1029/2020JE006407

McCord, T. B., Hansen, G. B., Matson, D. L., Johnson, T. V., Crowley, J. K., Fanale, F. P., et al. (1999). Hydrated salt minerals on Europa's surface from the Galileo near-infrared mapping spectrometer (NIMS) investigation. *Journal of Geophysical Research*, *104*(E5), 11827–11851. https://doi.org/10.1029/1999JE900005

Nimmo, F., & Gaidos, E. (2002). Strike-slip motion and double ridge formation on Europa. *Journal of Geophysical Research*, *107*(E4), 5021. https://doi.org/10.1029/2000JE001476

Nimmo, F., Pappalardo, R., & Giese, B. (2003). On the origins of band topography, Europa. *Icarus*, *166*(1), 21–32. https://doi.org/10.1016/j.icarus.2003.08.002

Nimmo, F., & Pappalardo, R. T. (2016). Ocean worlds in the outer solar system. *Journal of Geophysical Research: Planets*, *121*(8), 1378–1399. https://doi.org/10.1002/2016JE005081

Orlando, T. M., McCord, T. B., & Grieves, G. A. (2005). The chemical nature of Europa surface material and the relation to a subsurface ocean. *Icarus*, *177*(2), 528–533. https://doi.org/10.1016/j.icarus.2005.05.009

Pappalardo, R. T., Belton, M. J. S., Breneman, H. H., Carr, M. H., Chapman, C. R., Collins, G. C., et al. (1999). Does Europa have a subsurface ocean? Evaluation of the geological evidence. *Journal of Geophysical Research*, *104*(E10), 24015–24055. https://doi.org/10.1029/1998JE000628

Pappalardo, R. T., Head, J. W., Greeley, R., Sullivan, R. J., Pilcher, C., Schubert, G., et al. (1998). Geological evidence for solid-state convection in Europa's ice shell. *Nature*, *391*(6665), 365–368. https://doi.org/10.1038/34862

Petit, J. P. (1987). Criteria for the sense of movement on fault surfaces in brittle rocks. *Journal of Structural Geology*, *9*(5–6), 597–608. https://doi.org/10.1016/0191-8141(87)90145-3

Postberg, F., Grün, E., Horanyi, M., Kempf, S., Krüger, H., Schmidt, J., et al. (2011). Compositional mapping of planetary Moons by mass spectrometry of dust ejecta. *Planetary and Space Science*, *59*(14), 1815–1825. https://doi.org/10.1016/j.pss.2011.05.001

Prockter, L. M., Antman, A. M., Pappalardo, R. T., Head, J. W., & Collins, G. C. (1999). Europa: Stratigraphy and geological history of the anti-Jovian region from Galileo E14 solid-state imaging data. *Journal of Geophysical Research*, *104*(E7), 16531–16540. https://doi.org/10.1029/1998JE001015

Prockter, L. M., Head, J. W., Pappalardo, R. T., Sullivan, R. J., Clifton, A. E., Giese, B., et al. (2002). Morphology of Europan bands at high resolution: A mid-ocean ridge-type rift mechanism. *Journal of Geophysical Research*, *107*(E5), 5028. https://doi.org/10.1029/2000JE001458

Prockter, L. M., & Pappalardo, R. T. (2000). Folds on Europa: Implications for crustal cycling and accommodation of extension. *Science*, *289*(5481), 941–943. https://doi.org/10.1126/science.289.5481.941

Prockter, L. M., Pappalardo, R. T., & Head, J. W. (2000). Strike-slip duplexing on Jupiter's icy moon Europa. *Journal of Geophysical Research*, *105*(E4), 9483–9488. https://doi.org/10.1029/1999JE001226

Prockter, L. M., & Patterson, G. W. (2009). Morphology and evolution of Europa's ridges and bands. In *Europa* (pp. 237–258). https://doi.org/10.2307/j.ctt1xp3wdw.16

Quick, L. C., & Marsh, B. D. (2015). Constraining the thickness of Europa's water–ice shell: Insights from tidal dissipation and conductive cooling. *Icarus*, *253*, 16–24. https://doi.org/10.1016/j.icarus.2015.02.016

Rhoden, A. R., Mohr, K. J., Hurford, T. A., Henning, W., Sajous, S., Patthoff, D. A., & Dubois, D. (2021). Obliquity, precession, and fracture mechanics: Implications of Europa's global cycloid population. *Journal of Geophysical Research: Planets*, *126*(3), e2020JE006710. https://doi.org/10.1029/2020JE006710

Rossi, C., Cianfarra, P., Salvini, F., Bourgeois, O., & Tobie, G. (2020). Tectonics of Enceladus' South Pole: Block rotation of the Tiger stripes. *Journal of Geophysical Research: Planets*, *125*(12), 1–21. https://doi.org/10.1029/2020JE006471

Rossi, C., Cianfarra, P., Salvini, F., Mitri, G., & Massé, M. (2018). Evidence of transpressional tectonics on the Uruk Sulcus region, Ganymede. *Tectonophysics*, *749*(March), 72–87. https://doi.org/10.1016/j.tecto.2018.10.026

Sarid, A. (2002). Polar wander and surface convergence of Europa's Ice Shell: Evidence from a survey of strike-slip displacement. *Icarus*, *158*(1), 24–41. https://doi.org/10.1006/icar.2002.6873

Schenk, P., Matsuyama, I., & Nimmo, F. (2008). True polar wander on Europa from global-scale small-circle depressions. *Nature*, *453*(7193), 368–371. https://doi.org/10.1038/nature06911

Schenk, P., Matsuyama, I., & Nimmo, F. (2020). A very young age for true polar wander on Europa from related fracturing. *Geophysical Research Letters*, *47*(17), 1–9. https://doi.org/10.1029/2020GL088364

Schenk, P. M. (2002). Thickness constraints on the ice shells of the Galilean satellites from a comparison of crater shapes. *Nature*, *417*(6887), 419–421. https://doi.org/10.1038/417419a

Schenk, P. M., & Pappalardo, R. T. (2004). Topographic variations in chaos on Europa: Implications for diapiric formation. *Geophysical Research Letters*, *31*(16), 1–5. https://doi.org/10.1029/2004GL019978

Schmidt, B. E., Blankenship, D. D., Patterson, G. W., & Schenk, P. M. (2011). Active formation of "chaos terrain" over shallow subsurface water on Europa. *Nature*, *479*(7374), 502–505. https://doi.org/10.1038/nature10608

Schmidt, G., Luzzi, E., Rossi, A. P., Pondrelli, M., Apuzzo, A., & Salvini, F. (2022). Protracted hydrogeological activity in Arabia Terra, Mars: Evidence from the structure and mineralogy of the layered deposits of Becquerel crater. *Journal of Geophysical Research: Planets*, *127*(9), e2022JE007320. https://doi.org/10.1029/2022JE007320

Schubert, G., Sohl, F., & Hussmann, H. (2009). Interior of Europa. *Europa*, 353–367.

Singer, K. N., McKinnon, W. B., & Nowicki, L. T. (2013). Secondary craters from large impacts on Europa and Ganymede: Ejecta size–velocity distributions on icy worlds, and the scaling of ejected blocks. *Icarus*, *226*(1), 865–884. https://doi.org/10.1016/j.icarus.2013.06.034

Singer, K. N., McKinnon, W. B., & Schenk, P. M. (2021). Pits, uplifts and small chaos features on Europa: Morphologic and morphometric evidence for intrusive upwelling and lower limits to ice shell thickness. *Icarus*, *364*, 114465. https://doi.org/10.1016/j.icarus.2021.114465

Sotin, C., Tobie, G., Wahr, J., McKinnon, W. B., McKinnon, W. B., & Khurana, K. K. (2009). Tides and tidal heating on Europa. *Europa*, *11*.

Thaller, T. F. (2000). Galileo orbital operations solid state imaging raw EDR V1.0. [Dataset]. NASA Planetary Data System. https://doi.org/10.17189/1520425

Trumbo, S. K., Becker, T. M., Brown, M. E., Denman, W. T. P., Molyneux, P., Hendrix, A., et al. (2022). A new UV spectral feature on Europa: Confirmation of NaCl in leading-hemisphere chaos terrain. *The Planetary Science Journal*, *3*(2), 27. https://doi.org/10.3847/PSJ/ac4580

Trumbo, S. K., Brown, M. E., Fischer, P. D., & Hand, K. P. (2017). A new spectral feature on the trailing hemisphere of Europa at 3.78 μ m. *The Astronomical Journal*, *153*(6), 250. https://doi.org/10.3847/1538-3881/aa6d80

Trumbo, S. K., Brown, M. E., & Hand, K. P. (2019a). $H_2 O_2$ within chaos terrain on Europa's leading hemisphere. *The Astronomical Journal*, *158*(3), 127. https://doi.org/10.3847/1538-3881/ab380c

Trumbo, S. K., Brown, M. E., & Hand, K. P. (2019b). Sodium chloride on the surface of Europa. *Science Advances*, *5*(6), 2–6. https://doi.org/10.1126/sciadv.aaw7123

Tufts, B. R., Greenberg, R., Hoppa, G., & Geissler, P. (1999). Astypalaea linea: A large-scale strike-slip fault on Europa. *Icarus*, *141*(1), 53–64. https://doi.org/10.1006/icar.1999.6168

Tufts, B. R., Greenberg, R., Hoppa, G., & Geissler, P. (2000). Lithospheric dilation on Europa. *Icarus*, *146*(1), 75–97. https://doi.org/10.1006/icar.2000.6369

Vance, S., Harnmeijer, J., Kimura, J., Hussmann, H., DeMartin, B., & Brown, J. M. (2007). Hydrothermal systems in small ocean planets. *Astrobiology*, *7*(6), 987–1005. https://doi.org/10.1089/ast.2007.0075

Vance, S. D., Hand, K. P., & Pappalardo, R. T. (2016). Geophysical controls of chemical disequilibria in Europa. *Geophysical Research Letters*, *43*(10), 4871–4879. https://doi.org/10.1002/2016GL068547